NASA Technical Memorandum 87038

Operating Characteristics of a 0.87 kW-hr Flywheel Energy Storage Module

Stuart H. Loewenthal, Herbert W. Scibbe,
Richard J. Parker, and Erwin V. Zaretsky
Lewis Research Center
Cleveland, Ohio

Prepared for the
20th Intersociety Energy Conversion Engineering Conference (IECEC)
cosponsored by the SAE, ANS, ASME, IEEE, AIAA, ACS, and AIChE
Miami Beach, Florida, August 18-23, 1985

NASA

ABSTRACT

Discussion is given of the design and loss characteristics of 0.87 kW-hr (peak) flywheel energy storage module suitable for aerospace and automotive applications. The maraging steel flywheel rotor, a 46-cm- (18-in-) diameter, 58-kg (128-lb) tapered disk, delivers 0.65 kW-hr of usable energy between operating speeds of 10 000 and 20 000 rpm. The rotor is supported by 20- and 25-mm bore diameter, deep-groove ball bearings, lubricated by a self-replenishing wick type lubrication system. To reduce aerodynamic losses, the rotor housing was evacuated to vacuum levels from 40 to 200 millitorr. Dynamic rotor instabilities uncovered during testing necessitated the use of an elastomeric-bearing damper to limit shaft excursions. Spindown losses from bearing, seal, and aerodynamic drag at 50 millitorr typically ranged from 64 to 193 W at 10 000 and 20 000 rpm, respectively. Discharge efficiency of the flywheel system exceeded 96 percent at torque levels greater than 21 percent of rated torque.

THE USE OF FLYWHEELS SPANS THE BREADTH of civilization from the ancient potter's wheel to advanced satellite control moment gyros. In the last 20 years or so, emphasis has been placed on the load leveling capability of flywheels as a means to save fuel or electrical energy for a wide variety of ground vehicles. These vehicles range from cars such as the British Gyreacta Flywheel transmissions developed in the 1950's (1)* and University of Wisconsin's flywheel powered 1980 Pontiac Phoenix (2) that demonstrated 100 percent increase in city mileage to flywheel electric vehicles. These also include the Airesearch battery-electric flywheel car (2) and transit buses such as the 1950's Swiss Oerlikon Electrogyro trolley (3) and more recently the Fiat, Volvo, M.A.N. gyro buses (4). A very innovative vehicle application is the recent, multi-disk, flywheel propulsion unit built by Rocketdyne to power coal mining shuttle cars without the need to pay out heavy electrical power cables (5).

Momentum wheels for satellite stabilization have been in general use since the late 50's. A more recent interest is to combine the energy storage capabilities of flywheels with their attitude control capabilities to form an integrated power/attitude control system (IPACS) for spacecraft (6). Research performed thus far on the IPACS concept indicates that a number of benefits can be realized by integrating these two functions including reduced size, weight, and cost as well as extended operational life and higher energy transfer rates relative to electrochemical storage systems (6). Although the technology to construct an acceptable IPACS system is basically in hand, a number of technical issues still require greater attention. One issue is the choice of material for rotor construction, that is, some type of composite fiber wrapped wheel versus a solid metal disk of high strength steel, titanium or metal matrix composites. A second concern is the type of bearing support system, that is, either active/-passive magnetic support or rolling-element bearing support.

Composite material wheels are generally favored over metal rotors because they have higher energy density potential and are thought to have a more benign failure mode. However the rotational speeds needed to realize this energy density advantage are about twice that of the metal rotor. This unfortunately puts a much greater burden on the support bearings, lubrication and sealing systems as well as heightens the possibility of rotor instability problems. Furthermore, tests on five different composite rotor designs were reported in Ref. 7 to fail

*Numbers in parentheses designate references at end of paper.

catastrophically either by complete disk burst or rim rupture.

Due to their noncontacting nature, magnetic rotor suspensions have the potential of long life, low losses, and very high speed capability. However, their need for rather sophisticated, multiaxis controls, lack of lateral stiffness, and the need for back up, touch down bearings in case of electronic component failure have limited their wide spread acceptance.

Metal wheels and conventional ball bearings are the proper baseline to gauge the performance potential of advanced composite rotors and magnetic suspension systems. Reliability levels associated with satellite gyro stabilization systems using this more conventional technology have been impressive. Some of these systems have performed flawlessly on earth orbiting spacecraft for as long as 7 years or more (8). Despite their widespread use as inertial stabilization systems since the late 50's, test data on the performance characteristics of metal flywheel energy storage modules for energy management applications are not abundant in the open literature. Engineering problems concerning the lubrication and temperature management of support bearings in a vacuum, the choice of sealing system, control of rotor dynamic instabilities, and the minimization of power loss still require close attention. The principal objective of this investigation is to quantify the extent of these problem areas and to identify possible promising approaches for improved performance.

FLYWHEEL MODULE DESCRIPTION

A cross section of the flywheel rotor test module appears in Fig. 1. The flywheel module consisted of a horizontally oriented, 58-kg (128-lb) maraging steel, tapered disk, supported by a pair of deep-groove ball bearings. The lower housing encapsulates the rotor and contains oil reservoirs for the support bearing's wick feed system. The upper housing contains a carbon face seal, drive spindle, and rotor release plunger to decouple the rotor from the rest of the drive system for the coast down tests.

General operating and design specifications for the flywheel module, support bearings, and rotor disk can be found in Tables I, II, and III respectively. A weight optimization of the flywheel module test package was not performed. Bearing system 10-percent life at a continuous 20 000 rpm is estimated to be in excess of 9000 hr. Based on a finite element analysis, the peak rotor stress at 20 000 rpm is ∿42 percent of the maraging steel's rated tensile strength and the peak fluctuating stress is about a third of the fatique limit at 1×10^8 cycles (Table III). These relatively conservative stress safety margins could probably be relaxed somewhat to provide greater energy storage capability if the need should arise.

The drive spindle was connected to a 2.48:1 spiral bevel gear, speed reducer gearbox mounted on top of the flywheel module housing (see Fig. 2). This right angle gearbox connected the rotor to the 150-kW eddy current brake (through shaft) and drive motor. The entire flywheel module test package was mounted inside a steel safety containment vessel.

A torque meter mounted between the module and the brake measured input and output torque levels. Thermocouples recorded temperatures on the support bearings' outer races, the ambient temperature within the vicinity of the rotor tip as well as other key component temperatures. Accelerometers mounted in x-y locations on the upper and lower support bearing cartridges tracked rotor vibration levels. These accelerometers together with x-y proximity probes mounted at the perimeter of the rotor disk were used to perform insitu balancing of the wheel assembly. They also gave performance data regarding the effectiveness of the elastomer bearing damper (see Fig. 1) which housed the upper support bearing.

A vacuum oil diffusion pump was used to evacuate the rotor enclosure. Absolute pressure levels down to 40 millitorr could be achieved during testing.

POWER TRANSFER TESTS

The electric drive motor was used to power the flywheel rotor up to full speed. The brake was then engaged at a preset torque level to determine the effectiveness of the rotor during energy change and discharge cycles.

A typical energy dissipation chart at three braking torque levels (measured by the output torque meter) for these tests appears in Fig. 3. The rate of rotor speed decay with time, α, is a direct measure of the torque being dissipated by the rotor, T_R, according to the following formula:

$$T_R = I\alpha$$

where I is the mass moments of inertia of the rotor as given in Table III.

The ratio of braking torque T_B to rotor torque T_R divided by the bevel gear set ratio of 2.48 is equal to the efficiency of the flywheel module system (rotor, support bearings, seal, bevel gear set, and drive spindle bearings) during discharge. For the measured speed decay curves of Fig. 3, discharge efficiency values were nominally 90, 93, and 96 percent at 10, 14, and 21 percent of the maximum rated discharge torque, respectively. The peak rated power delivery of 120 kW at 20 000 rpm corresponds to a maximum rated discharge torque of 57.0 N•m (504 in-lb). The bulk of these losses is due to the test stand bevel gear set assembly. To separate out these system losses from those of the flywheel rotor itself, coast down tests were performed on the rotor after being decoupled from the rest of the drive system.

COAST DOWN TEST RESULTS

An important issue for the application of flywheels as energy storage devices is their power consumption characteristics. Rotor bearing and rotor aerodynamic drag are two of the major contributors to these parasitic losses. To evaluate these losses, the rotor was charged up to its maximum speed of 20 000 rpm, the drive system release mechanism was actuated, and the rotor was freely allowed to coast down in speed. The absolute pressure in the rotor housing was varied to determine its effect on rotor windage losses and bearing temperatures.

As previously mentioned, charting rotor speed decay with time is an accurate means of assessing the parasitic drag torque losses. Results from three trial runs at each of three housing vacuum levels appear in Fig. 4. Parasitic losses at the lowest pressure were quite modest with the rotor still turning at about 7000 rpm after 8 hr from release.

Drag torque results that appear in Figs. 5(a) and (b) reflect the rotor system's parasitic loss characteristics. As one might suspect, both speed and pressure level have a substantial effect. For example, doubling the rotor speed approximately triples the power loss while reducing housing pressure from about 200 to 50 millitorr cuts the losses almost in half.

It is instructive to sort out the loss contributions from the support bearings from those due to the rotor windage drag. A rough estimate of windage losses can be found from the plot of total drag torque versus absolute housing pressure appearing in Fig. 6. The marked reduction in drag torque with a reduction in housing pressure is largely due to a reduction in the density of air surrounding the rotor and its subsequent effect on the aerodynamic drag of the rotor. A secondary effect is that the bearings will operate at cooler temperatures when the housing pressure is low (see Fig. 7) since the aerodynamic heating of the rotor is less.

It is clear from Fig. 6 that reducing the absolute housing pressure from 195 to 45 millitorr will approximately halve the total parasitic drag. This implies that the rotor windage losses probably account for more than half of the total measured losses. Figure 6 also suggests that reducing the housing pressure below 45 millitorr will cause a further reduction in parasitic losses. However the extent of this reduction is not known.

BEARING TEMPERATURES - A significant concern to those who design vacuum contained momentum wheels is providing a means to properly lubricate and cool the support bearings. Since convective cooling is unavailable, bearing temperature management is primarily limited to conductive heat transfer and minimization of bearing heat generation through adequate but not excessive liquid lubrication.

In Ref. 9 the pressurized oil-jet lubrication system for the rotor support bearings was found to deliver excessive quantities of oil. Flow rates above 20 cc/min caused a rapid torque increase with speed. It was necessary to cut flow rates down to 5 to 13 cc/min to produce stable (nonerratic) bearing rotation torque traces.

In view of the low bearing flow rates identified in Ref. 9, it was judged that a recirculating type, cotton wick feed system could provide sufficient lubrication to the bearing and in a very simple manner. A lightly spring loaded wick, saturated with oil, contacts a conical sleeve adjacent to the bearing inner race. Frictional contact against the sleeve causes a small amount of oil to be deposited. This oil migrates along the sleeve to its large end and into the bearing under the centrifugal force field. The wick absorbs oil from the reservoir which travels through the wick by capillary action to replenish the oil entering the bearing. Oil droplets leaving the bearing and oil vapor which coalesce against the cooler housing walls eventually return to the reservoir, thus closing the cycle.

The bearing outer race temperature profiles shown in Fig. 7 confirm that the wick feed system provide adequate cooling, particularly at the lower vacuum levels. Because of the large mass associated with the rotor and structure which surrounds the bearing, temperature data at the higher speeds had insufficient time from rotor release to reach steady state values. It appears that ∿2 hr of coast down time is required (see Fig. 4 for speed versus time values) to reach the steady state portion of the temperature curves. An extrapolation of these steady state temperature trends of Fig. 7 to the higher speeds will give an estimate of the maximum expected bearing temperatures. These maximum temperatures are reasonably low for the lower housing pressure levels (below 105 millitorr). However at the 190 to 200 millitorr level, aerodynamic heating of the rotor will soak back into the bearings, elevating the maximum temperature at the higher speeds. Power tests in which the rotor was driven to a speed of 15 000 rpm while the housing was vented to atmospheric pressure heated the air surrounding the rotor to a temperature of 100 °C (211 °F) in as little as 10 minutes of operation. This test-rotor dissipates ∿9 kW of power at 15 000 rpm at ambient pressure and temperature according to the following windage loss expression derived in Ref. 10 from turbine disk spin loss data. The power loss P in kW of a cylindrical disk of radius R and thickness t in meters is given by:

$$P_W = 2.04\times10^{-8}\left(1 + 2.3\,\frac{t}{R}\right)\rho^{0.8}\mu^{0.2}R^{4.6}n^{2.8}$$

where ρ is the air density in kg/m^3, μ is abolute air viscosity in cP and n is disk speed in rpm.

It is obvious from the above expression that windage losses are quite sensitive to

speed. For example, doubling rotor speed, which may be appropriate for a composite material rotor, will cause a seven fold loss increase in ambient air. The validity of this expression has not been established in a vacuum where molecular rather than viscous air flow occurs. However, if the validity of this relation does hold, then about an eleven fold reduction in housing pressure would be needed to offset this doubling of speed. Thus sealing requirements for composite rotors are significantly more demanding than those for metal rotors. This is not only due to the need to keep drag losses to a minimum but also to prevent aerodynamic heating of the composite material that leads to a loss in fiber/resin strength.

BEARING TESTS

The bearing test rig shown in Fig. 8 was used to investigate the torque and temperature characteristics of the rotor support bearings. Both standard and high radial clearance ball bearings of 20- and 25-mm bore diameter were tested under 445 N (100 lb) and 890 N (200 lb) loads with three different oils (SAE 10, MIL-L-7808, gyro oil SRG-30) and one vacuum grease (ANDOK-C). Those bearing tests were conducted prior to the tests with the flywheel module in order to select the best oil and clearance combination for the rotor bearings.

The test bearing was mounted on the turbine spindle shaft inside the vacuum chamber. The outer race was pressed into a freely suspended bearing cartridge which contained the bearing oil reservoir. Bearing thrust loads were provided by a dead weight jacket which pulled against the bearing cartridge but was not allowed to contact the inside of the vacuum chamber. The bearing cartridge and dead weight assembly was prevented from rotating by a reaction torque cell which provided a direct measurement of the bearing drag torque. The bearing was lubricated by a wick feed system similar to that used in the flywheel module. Bearing outer race temperatures were obtained from thermocouples mounted against the test bearing outer race.

BEARING TEST RESULTS - Torque and temperature data for the 20-mm bore diameter lower rotor bearing appears in Fig. 9. During these tests bearing speed was stepped up from 10 000 to 15 000 to 18 000 rpm in 30-min increments and finally to 20 000 rpm which was maintained for a total of 90 min. As can be seen from the data, bearing torque and temperature approached, but did not achieve steady-state values at the end of these time intervals, except for the 20 000 rpm data.

Bearing outer race temperatures shown in Fig. 9 are generally higher than those from the flywheel module tests (Fig. 7). The principal reason is believed due to the difference in heat flow paths. The heat conduction path for the flywheel module bearings is directly through the housing structure which is cooled by the ambient air. On the other hand, the test bearing in the bearing tester (Fig. 8) is surrounded by structure which is also suspended in the vacuum. Thus the only heat conduction path to the outer housing is restricted to that passing through the torque cell. Although the bearing loads in the microgravity environment of space will be considerably lower than those investigated here, bearing temperature management is still a concern because of the lack of convective cooling.

Lighter bearing loads not only reduce operating temperatures but cause an appreciable reduction in bearing drag torque as well as extend bearing life. For example, cutting test bearing thrust loads from 890 N (200 lb) to 445 N (100 lb) reduced outer race temperature by 14 °C (25 °F) and bearing torque by about 20 percent at 20 000 rpm according to Fig. 9.

At 20 000 rpm, bearing torques ranged from about 35 N•mm (5 oz-in) at the lighter load to about 42 N•mm (6 oz-in) at the heavier load. At 10 000 rpm these torque values are approximately 42 N•mm (6 oz-in) and 54 N•mm (7.6 oz-in), respectively. Apparently the cooler operating temperatures encountered at the lower speeds caused bearing torque to be larger than those measured at the higher speeds. However, bearing torque appears to be generally insensitive to shaft speed. This is indicativ of a bearing which is not excessively lubricated. Excessive lubrications would cause a rapid increase in both torque and temperature with speed.

Although not shown, test results for the 25-mm bore, upper support bearing were quite similar to those of Fig. 9 at the same loads and speeds. With the exception of the MIL-L-7808 oil, the choice of test lubricant from those investigated did not have a marked effect on either bearing torque or temperature. The 7808 oil produced unstable operating conditions at the higher speeds which lead to thermal failures. In general, an increase in bearing radial clearance from nominally 0.018/0.020 mm (0.0007/0.0008 in) to 0.028/0.033 mm (0.0011/-0.0013 in) had no consistently significant effect on either bearing temperatures or torques.

ROTOR DYNAMICS

Because of the large mass associated with the flywheel it was expected that at least one critical speed would be encountered before the rotor would reach its maximum rated speed of 20 000 rpm. A critical speed analysis was performed on the rotor/wheel system. The results of this analysis appear in Fig. 10. The first natural frequency was found to be dependent on bearing stiffness. It was likely to be encountered at speeds above 7000 rpm for a "hard mounted" bearing system. The stiff, short rotor shaft ensured that the second critical speed was relatively insensitive to bearing stiffnesses and occurred at rotor

speeds of 55 000 rpm or greater. This is more than twice the maximum rated speed of the wheel.

Early tests with the flywheel module did in fact uncover high vibration levels acting on the support bearings as the speed approached the 10 000 rpm and beyond. These dynamic loads became so severe that bearing temperatures quickly rose. Rotor test speeds had to be limited to 15 000 rpm to avoid overheating and subsequent failure of the support bearings. In situ balancing of the rotor assembly was not helpful.

BEARING DAMPER - A spring-squeeze film bearing damper was designed to dissipate some of the dynamic energy of the rotor and help limit shaft excursions. The damper ring, which was fitted over the bearing outer race had a slightly smaller diameter than the housing bore. Four 2.4-mm- (0.094-in-) diameter pins, brazed in holes drilled in the axial face of the damper ring, centered it within the housing bore. These pins provided a spring deflection. The clearance between the damper ring and the housing trapped oil which was "squeezed" when the damper deflected, thereby providing viscous damping. However, after repeated attempts, the authors were unable to find the right pin diameter for this damper spring to permit sufficient deflection for damping without being too weak in flexural fatigue. Two different squeeze film damper designs failed in service at about 15 000 rpm with little more than superficial damage to either the flywheel rotor or housing.

As an alternate, an elastomeric damper was finally adopted. As shown in Fig. 1, the damper consists of a bearing damper sleeve circumscribed by two 70 durometer, rubber O-rings. The bearing sleeve is lightly pressed into the housing bore to provide about 0.08 mm (0.003 in) of O-ring radial deformation for elastomeric damping.

This elastomer damper design provided satisfactory performance throughout the operating speed range. A nonsynchronous (total) component vibration plot from accelerometers attached to the upper and lower bearing mounts appears in Fig. 11. A noticeable rise in acceleration levels between 5200 to 5400 rpm is evident. This is probably indicative of the rotor system's first critical speed. No other vibration excursion was found over the operating speed range. Since this plot contains vibration information from the surrounding structural components at all frequencies, not just those at the rotor speed (so-called synchronous vibration), it is not possible to positively identify this region as a critical speed. However the likelyhood is high. Assuming this is the case, the elastomer damper appears to effectively limit the excursion in G-level at this speed based on the vibration trace in Fig. 11. The effective radial stiffness of the upper bearing damper system is probably less than about 53 000 N/cm (30 000 lb/in) based on the critical speed analysis shown in Fig. 10. In actuality, the damper stiffness is highly nonlinear, being relatively low at first and increasing rapidly as the O-ring is compressed. The initial stiffness is largely dictated by the installed fit up between the O-rings and housing bore.

The steady increase in vibration levels with speed shown in Fig. 11 is not a great concern. The acceleration data at the higher speeds are mainly comprised of the higher structural component resonant frequencies which are not particularly troublesome. They would be a concern if these same vibration levels had occurred at the lower rotor speeds.

CONCLUSION

Tests were performed on a 0.87 kW-hr flywheel energy storage module containing a 59-kg (130-lb), 46-cm (18-in-) diameter maraging steel rotor. Power delivery tests were conducted to determine system discharge efficiencies. Support bearing torque and temperature characteristics were determined from coast down tests from 20 000 rpm at three housing pressures levels of nominally 45, 95, and 195 millitorr. The upper rotor bearing was housed in an elastomer damper sleeve which was effective in reducing the dynamic loads acting on the support bearings. Without this damper, tests were limited to a maximum of 15 000 rpm. Based on a critical speed analysis as later confirmed by tests, no critical speeds were found in the 10 000 to 20 000 rpm operating range. Prior to the flywheel rotor coast down tests, support bearing tests were performed on a vacuum-equipped bearing tester to determine the effectiveness of the wick lubrication feed system.

The following results were obtained.

1. Total rotor parasitic losses can be cut in half by reducing housing pressure from approximately 200 to 50 millitorr. At 50 millitorr, these losses were approximately 64 and 193 W at 10 000 and 20 000 rpm, respectively.

2. Measured discharged efficiencies for the complete flywheel module increased with delivered torque, being 96 percent at 21 percent of maximum rated torque.

3. The wick feed system is a simple, but effective means of lubricating the rotor support bearings.

4. An elastomer bearing damper provided a significant reduction in bearing dynamic vibration loads. The damper's lower radial stiffness suppressed the system first critical speed well below the rotor's minimum operating speed of 10 000 rpm. No critical speeds were found in the 10 000 to 20 000 rpm design operating range.

REFERENCES

1. R.C. Clerk, "The Utilization of Flywheel Energy." SAE Trans., Vol. 72, 1964, pp. 508-543.

2. D.V. Edson, "Researchers Advance Heat Engine/Flywheel Technology." Design News, Vol. 36, Sept. 8, 1980, pp. 127-140.
3. "Oerlikon Electrogyro." Automobile Engineer, Vol. 45, No. 13, Dec. 1955, pp. 559-566.
4. D. Scott, and J. Yamaguchi, "Flywheel Buses Advance in Europe." Automotive Engineering, Vol. 88, No. 12, Dec. 1980, pp. 86-92.
5. D.V. Edson, "Breakthrough in Flywheel Technology." Science Mechanics, Mar/Apr 1984, pp. 33-35, 104-105, 109.
6. C.R. Klecker, R.J. Bechtel, and N.J. Groom, eds., "An Assessment of Integrated Flywheel System Technology." NASA-CP-2346, 1984.
7. A.P. Coppa, "Flywheel Containment and Safety Considerations." In An Assessment of Integrated Flywheel Systems Technology, NASA-CP-2346, 1984, pp. 243-264.
8. W. Auer, "Ball Bearing Versus Magnetic Bearing Reaction and Momentum Wheels as Momentum Actuators." Proceedings of the 14th Aerospace Mechanisms Symposium, NASA-CP-2127, 1980, pp. 79-91.
9. D.A. Wildermuth, "Spin Testing of Flywheel Bearings and Seal." LMC-760901-A, Lloyds Register of Shipping, London, Sept. 30, 1976.
10. N.E. Anderson, and S.H. Loewenthal, "Spur-Gear-System Efficiency at Part and Full Load." NASA-TP-1622, 1980.

Table I. - Flywheel Module Specifications

Operating speed range, rpm	10 000 to 20 000
Rated energy storage, W-hr (hp-min)	659 (52.4)
Peak energy storage, W-hr (hp-min)	869 (69.9)
Maximum rated power delivery kW (hp)	120 (160)
Absolute housing pressure, millitorr	40 to 200
Total flywheel module weight, kg (lb) (including 2.48:1 bevel gearbox)	221 (486)
Rotor weight, kg (lb)	58 (128)

Table II. - Rotor Support Bearings Specifications

Type	Deep-groove ball bearing
Cage	2-piece, machined phenolic
Size, upper/lower	105/204
Total radial clearance, mm (in)	0.033 (0.0013)
Lubricant system type	cotton wick feed
Lubricant	Mineral oil, fully formulated
Kinematic viscosity, cS	69 at 38 °C 8.4 at 100 °C
Bearing preload washer load, N (lb)	156 (35)
Bearing system life, hr (L_{10} at 20 000 rpm continuous)	9380

Table III. - Flywheel Rotor Disk Specifications

Diameter, cm (in)	46 (18)
Tip/hub width, cm (in)	3.8/5.1 (1.5/2.0)
Weight, kg (lb)	58.2 (128)
Mass moment of inertia, kg-m-sec^2 (lb-in-sec^2)	0.146 (12.62)
Material	Maraging steel, 5 percent chrome, R_c = 54
Yield strength, GPa (ksi)	1.62 (235)
Ultimate tensile strength, GPa (ksi)	2.00 (290)
Fatigue limit at 1×10^8 cycles, GPa (ksi)	±0.90 (±130)
Peak rotor tensile strength at center line, GPA (ksi)	0.848 (123)
Burst speed, rpm	30 700
Amplitude of maximum fluctuating stress, GPa (ksi)	±0.318 (±46.1)
Fatigue life, discharge cycles.	1×10^8

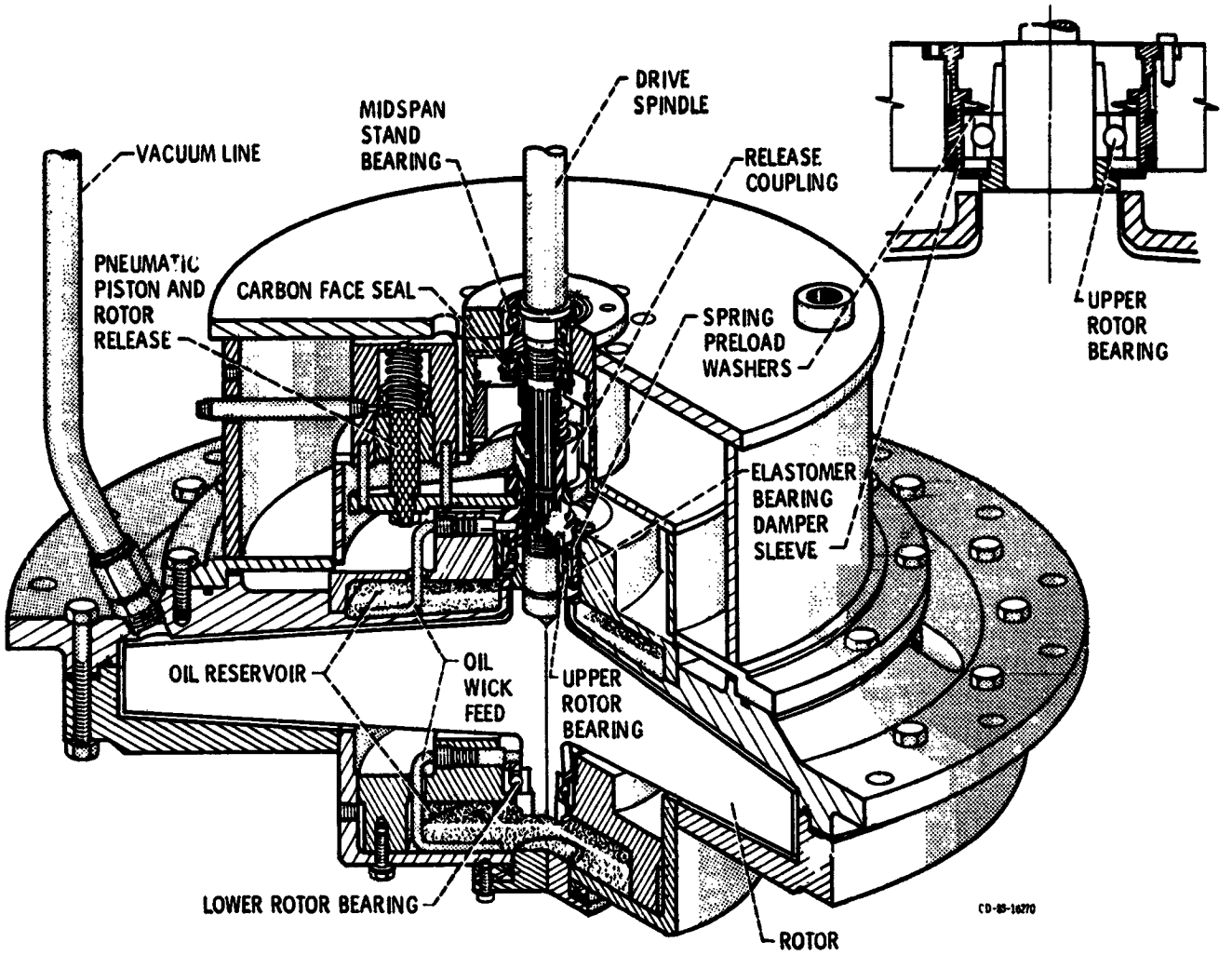

Fig. 1 - Schematic of NASA flywheel rotor module.

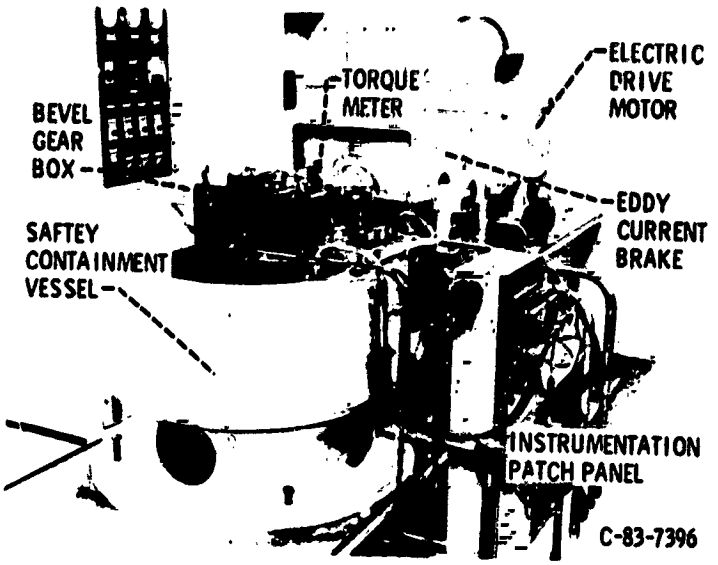

Fig 2. - Flywheel module test stand.

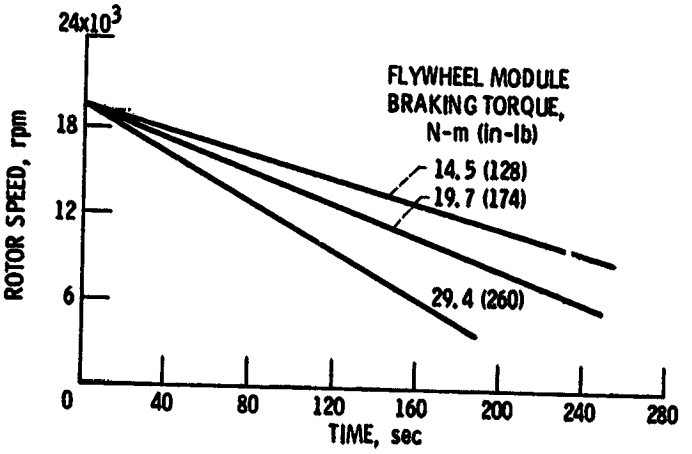

Fig. 3 - Flywheel rotor speed decay results from power discharge tests. Absolute housing pressure, ~70 millitorr.

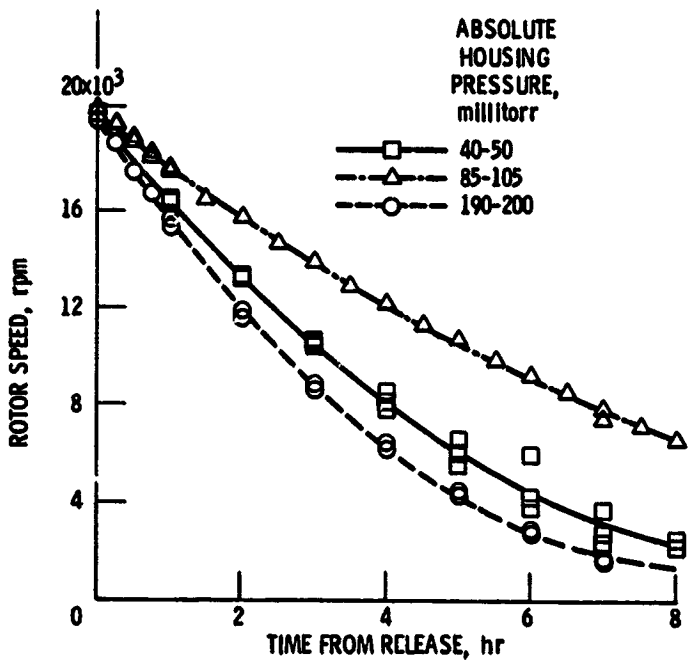

Fig. 4 - Flywheel rotor speed decay with time under coastdown.

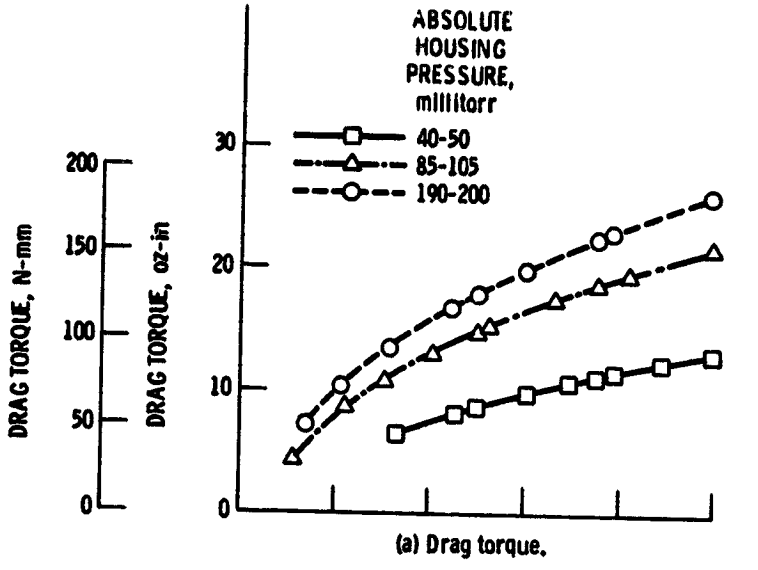

(a) Drag torque.

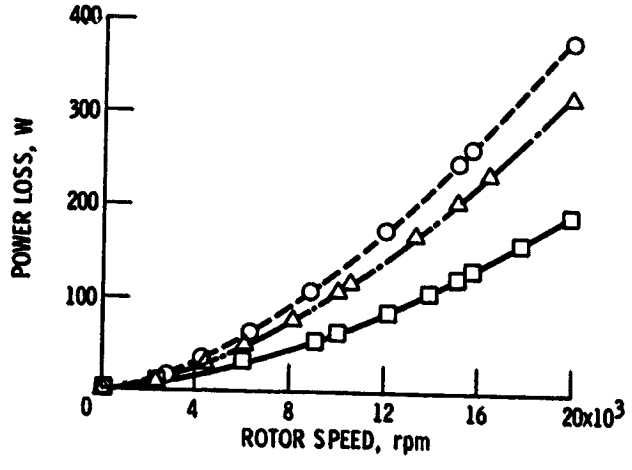

(b) Power loss.

Fig. 5 - Drag torque and power loss characteristics of NASA flywheel rotor under coastdown.

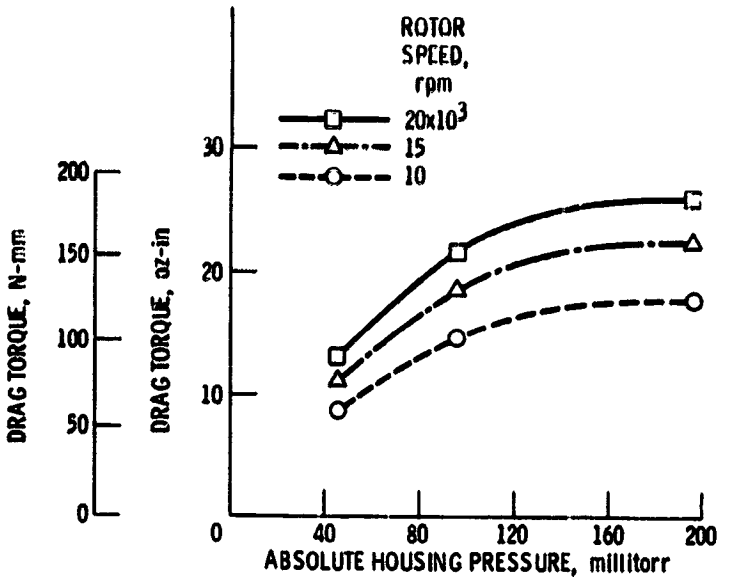

Fig. 6 - Effect of pressure on coastdown drag torque.

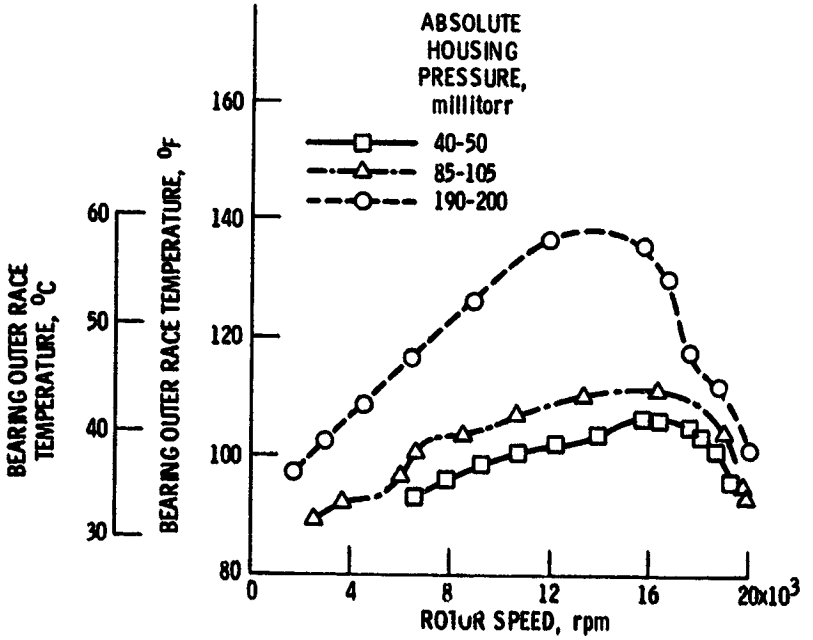

Fig. 7 - Rotor lower support bearing temperature characteristics with speed and housing pressure. (20-mm-bore deep-groove ball bearing under approx. 160-lb thrust load.)

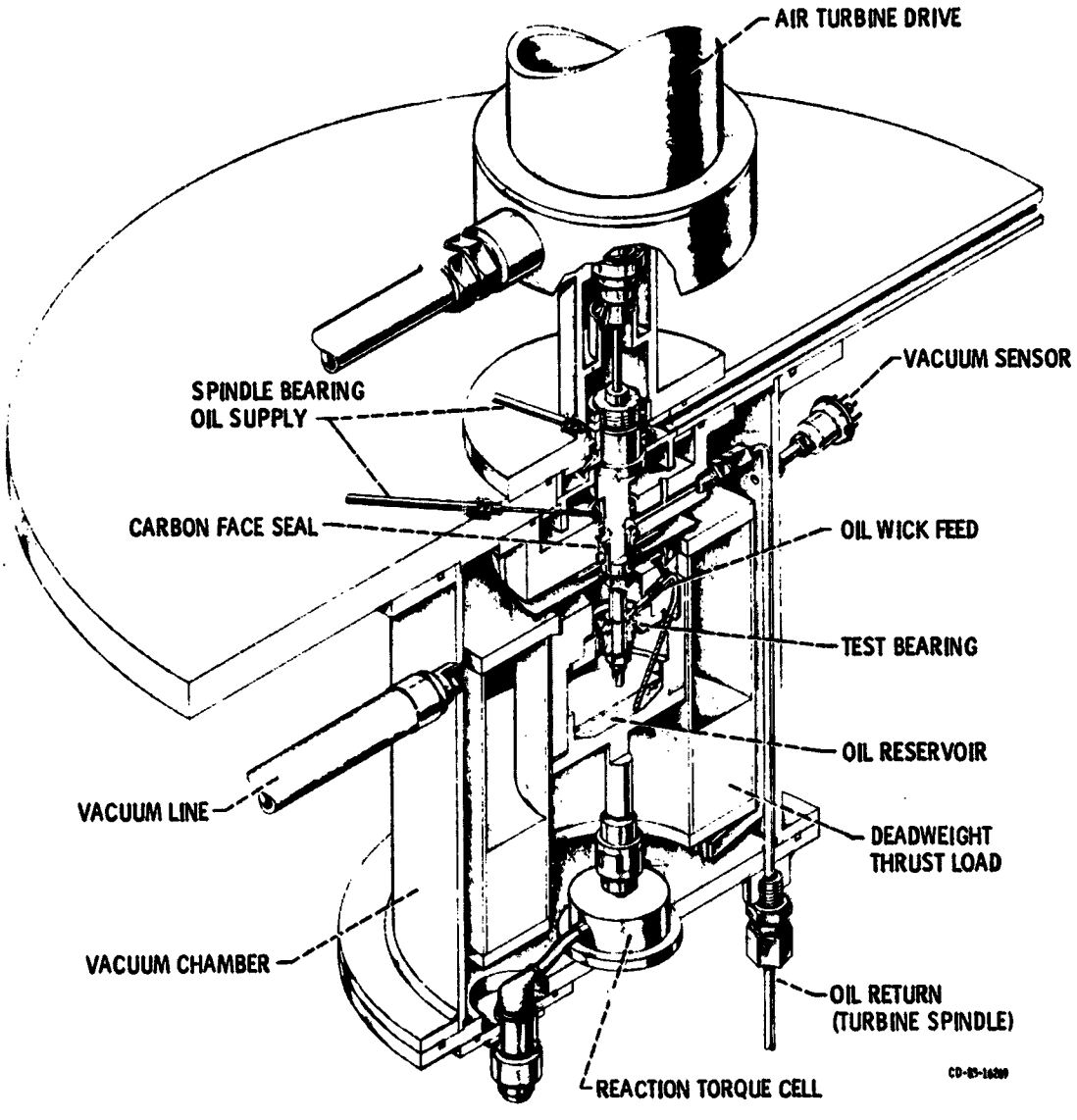

Fig. 8 - High-speed vacuum rotor bearing test rig.

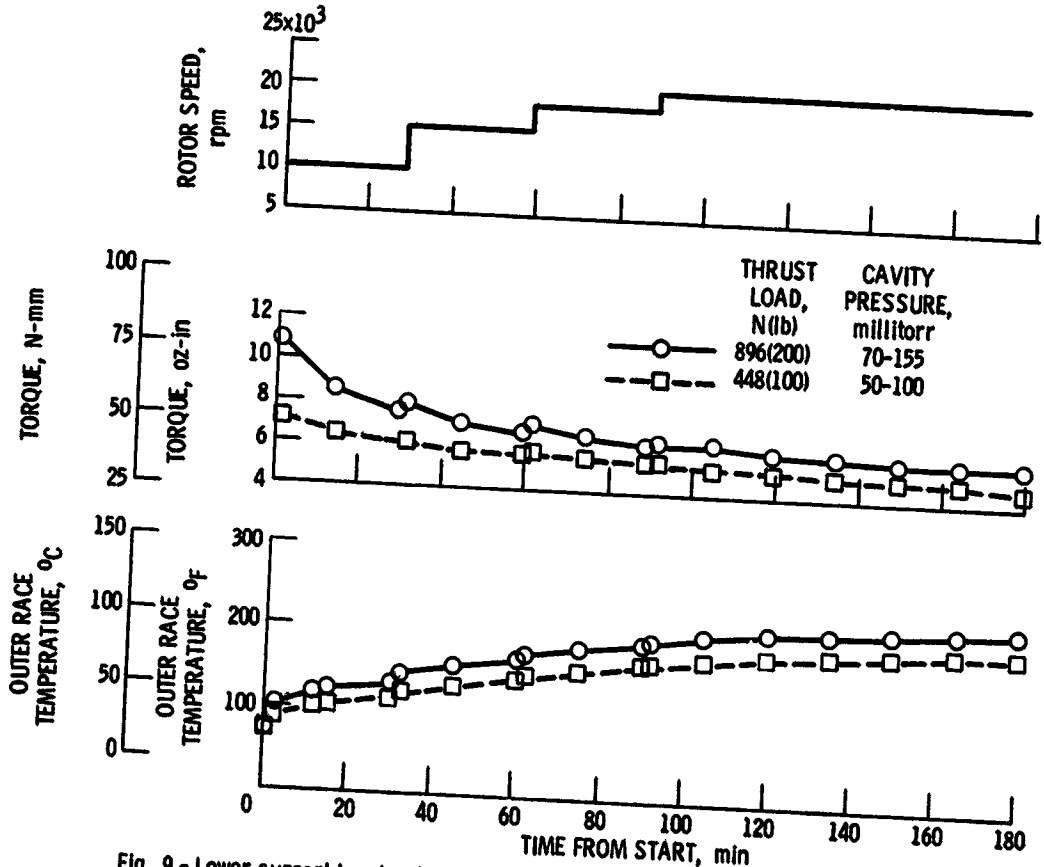

Fig. 9 - Lower support bearing torque and temperature characteristics from vacuum bearing tester. (20-mm bore, deep-groove ball bearing; 0.028-mm-radius clearance; wick lubricated with SAE-10 mineral oil.)

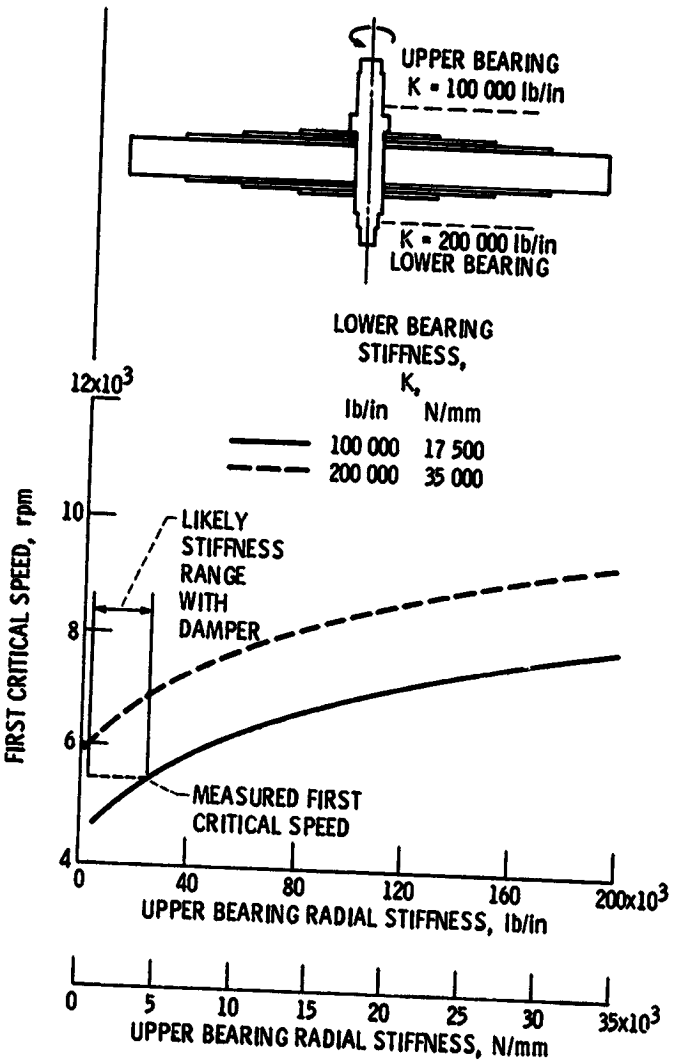

Fig. 10 - Critical speed analysis of NASA flywheel rotor. (Second critical rotor speed, >55 000 rpm for all upper bearing stiffnesses.)

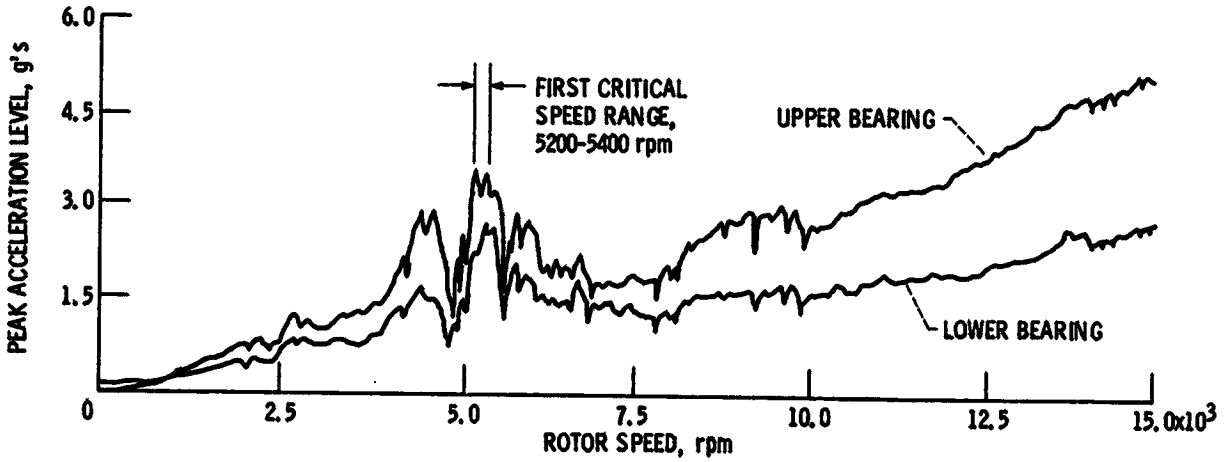

Fig. 11 - Total (nonsynchronous) vibration at bearing supports as function of rotor speed.

1. Report No.	2. Government Accession No.	3. Recipient's Catalog No.
NASA TM-87038		

4. Title and Subtitle	5. Report Date
Operating Characteristics of a 0.87 kW-hr Flywheel Energy Storage Module	6. Performing Organization Code: 505-33-7A

7. Author(s)	8. Performing Organization Report No.
Stuart H. Loewenthal, Herbert W. Scibbe, Richard J. Parker, and Erwin V. Zaretsky	E-2535
	10. Work Unit No.

9. Performing Organization Name and Address	11. Contract or Grant No.
National Aeronautics and Space Administration Lewis Research Center Cleveland, Ohio 44135	
	13. Type of Report and Period Covered: Technical Memorandum

12. Sponsoring Agency Name and Address	14. Sponsoring Agency Code
National Aeronautics and Space Administration Washington, D.C. 20546	

15. Supplementary Notes

Stuart H. Loewenthal, Richard J. Parker, and Erwin V. Zaretsky, NASA Lewis Research Center; Herbert W. Scibbe, currently with Goodyear Aerospace Corp., Akron, Ohio. Prepared for the 20th Intersociety Energy Conversion Engineering Conference (IECEC) cosponsored by the SAE, ANS, ASME, IEEE, AIAA, ACS, and AIChE, Miami Beach, Florida, August 18-23, 1985.

16. Abstract

Discussion is given of the design and loss characteristics of 0.87 kW-hr (peak) flywheel energy storage module suitable for aerospace and automotive applications. The maraging steel flywheel rotor, a 46-cm- (18-in-) diameter, 58-kg (128-lb) tapered disk, delivers 0.65 kW-hr of usable energy between operating speeds of 10 000 and 20 000 rpm. The rotor is supported by 20- and 25-mm bore diameter, deep-groove ball bearings, lubricated by a self-replenishing wick type lubrication system. To reduce aerodynamic losses, the rotor housing was evacuated to vacuum levels from 40 to 200 millitorr. Dynamic rotor instabilities uncovered during testing necessitated the use of an elastomeric-bearing damper to limit shaft excursions. Spindown losses from bearing, seal, and aerodynamic drag at 50 millitorr typically ranged from 64 to 193 W at 10 000 and 20 000 rpm, respectively. Discharge efficiency of the flywheel system exceeded 96 percent at torque levels greater than 21 percent of rated torque.

17. Key Words (Suggested by Author(s))	18. Distribution Statement
Flywheel; Ball bearings; Vacuum; Energy storage; Momentum wheels; Power loss	Unclassified - unlimited STAR Category 37

19. Security Classif. (of this report)	20. Security Classif. (of this page)	21. No. of pages	22. Price*
Unclassified	Unclassified		

*For sale by the National Technical Information Service, Springfield, Virginia 22161